J. Fluid Mech. (1996), *vol.* 317, *pp.* 195–214

Secondary flow in weakly rotating turbulent plane Couette flow

By KNUT H. BECH AND HELGE I. ANDERSSON

Faculty of Mechanical Engineering, Norwegian University of Science and Technology, N-7034 Trondheim, Norway

(Received 8 February 1995 and in revised form 8 February 1996)

As in the laminar case, the turbulent plane Couette flow is unstable (stable) with respect to roll cell instabilities when the weak background angular velocity $\Omega\hat{\boldsymbol{k}}$ is antiparallel (parallel) to the spanwise mean flow vorticity $(-\mathrm{d}U/\mathrm{d}y)\hat{\boldsymbol{k}}$. The critical value of the rotation number Ro, based on 2Ω and $\mathrm{d}U/\mathrm{d}y$ of the corresponding laminar flow, was estimated as 0.0002 at a low Reynolds number with fully developed turbulence. Direct numerical simulations were performed for $Ro = \pm 0.01$ and compared with earlier results for non-rotating Couette flow. At the low rotation rates considered, both senses of rotation damped the turbulence and the number of near-wall turbulence-generating events was reduced. The destabilized flow was more energetic, but less three-dimensional, than the non-rotating flow. In the destabilized case, the two-dimensional roll cells extracted a comparable amount of kinetic energy from the mean flow as did the turbulence, thereby decreasing the turbulent kinetic energy. The turbulence anisotropy was practically unaffected by weak spanwise rotation, while the secondary flow was highly anisotropic due to its inability to contract and expand in the streamwise direction.

1. Introduction

The study of turbulence in rotating reference frames is motivated by for example geophysical and turbomachinery applications. Investigations of the turbulent Reynolds stresses and their anisotropy are essential to improve the basic understanding and our ability to model the dynamics of such flows. The possible interaction between secondary flow and turbulence is hard to measure accurately in physical experiments, leaving direct numerical simulations as the appropriate method.

Turbulent channel flow with system rotation has been investigated both experimentally and numerically, see for example Johnston, Halleen & Lezius (1972) and Kristoffersen & Andersson (1993). Because of the (almost) symmetrical mean velocity profile in pressure-driven Poiseuille flow subject to slow system rotation, these investigators observed an anticyclonic side and a cyclonic side at which the turbulence was destabilized and stabilized, respectively. The background, or system, vorticity is parallel (anti-parallel) to the mean flow vorticity when the flow is cyclonic (anticyclonic). On the cyclonic side, the density of turbulence-generating events was reduced. In most cases, large-scale roll cells, or secondary vortices, aligned with the streamwise direction were found as secondary flows superimposed on the turbulence. The roll cells were asymmetric with respect to the centreline and originated on the destabilized side.

Similar roll cells also occur as a result of linear stability analysis of laminar rotating plane Poiseuille flow, see e.g. Alfredsson & Persson (1989). The physical origin of this instability is an imbalance between the pressure gradient and the Coriolis acceleration in the wall-normal direction. The corresponding stability problem for plane Couette flow is mathematically equivalent with the problem of thermal convection between two horizontal planes heated from below, see for example Lezius & Johnston (1976), in which the most unstable mode has a wavelength about twice the distance between the channel walls. The terms stable/unstable have a precise meaning in the case of laminar Couette flow. The laminar flow is unstable with respect to roll cell instabilities in the case of anticyclonic background vorticity of not too large magnitude, and stable in the case of cyclonic background vorticity. In the present contribution, this unambiguous definition of stable/unstable system rotation will be adopted, regardless of the effect of rotation on the turbulence.

The secondary flow set up by the Coriolis acceleration instability falls into the category known as Prandtl's first kind of secondary flow, cf. Bradshaw (1987), i.e. secondary flows caused by body forces (buoyancy, centrifugal, Coriolis). Prandtl's second kind of secondary flow is set up by spatial variation of the turbulent stresses that generate mean streamwise vorticity. Papavassiliou (1993) studied secondary vortices in numerically simulated non-rotating turbulent plane Couette flow, which were ascribed to the latter category of secondary flows. Even though the origin of these vortices was uncertain, it was found that the cross-sectional component of the secondary flow was sustained by correlations between turbulent stresses and secondary strain rates, i.e. an energy transfer from smaller to larger scales.

Smith & Townsend (1982) performed an experimental investigation of Taylor–Couette flow at relatively high Taylor numbers. Between the cylinders they observed toroidal eddies (secondary flow) with axial wavenumber quite similar to that found from stability analysis of the laminar flow. The secondary flow was more energetic than the residual turbulence. At the highest Taylor numbers, the toroidal eddies apparently became unstable. Watmuff, Witt & Joubert (1985) observed an array of vortex-like structures in developing turbulent boundary layers subject to system rotation. These large-scale structures were correlated with a spanwise variation of the skin friction. The experimental work of Bidokhti & Tritton (1992) on free shear layers with background rotation included measurements of the turbulence anisotropy. The cross-stream turbulence intensity was observed to increase with destabilizing rotation, while the streamwise intensity decreased. The Kelvin–Helmholtz instability roller eddies, with spanwise orientation, were destroyed by weak destabilizing rotation. Metais *et al.* (1992), and more recently Cambon *et al.* (1994) studied the effects of system rotation on large-scale vortices, superimposed on turbulence, using linearized theory and simulations of transient flows. Both investigations concluded that a slight anticyclonic background vorticity is destabilizing, while cyclonic background vorticity is stabilizing.

The main difference between pressure-driven channel flow and shear-driven Couette flow in this context is that the mean velocity profile of the latter is antisymmetric, i.e. the mean velocity distribution increases monotonically from one wall to the other and exhibits an inflection point at the centre. Both sides of the channel become either cyclonic or anticyclonic depending on the sense of rotation. This attractive feature of the rotating Couette flow facilitates the analysis and interpretation of the results. Similarities also exist between a free shear flow such as the turbulent mixing layer and the central region of the turbulent Couette flow. For both flows the mean velocity profile is inflectional and antisymmetric and the sign of the mean vorticity is

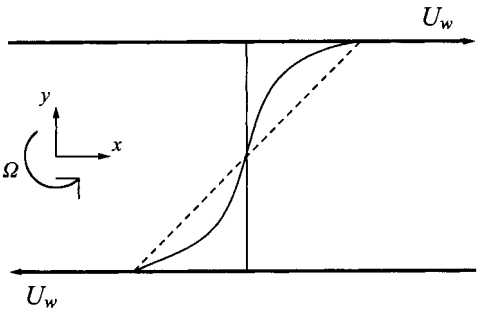

FIGURE 1. Sketch of rotating plane Couette flow. - - -, Laminar velocity profile; —, turbulent mean velocity profile.

unchanged. However, the inflection point corresponds to maximum mean vorticity in case of the mixing layer, whereas minimum vorticity coincides with the inflectional point of the Couette flow.

The objective of this paper is twofold: first to study the effect of weak system rotation in a fully turbulent channel flow where the imposed angular velocity is everywhere either parallel or anti-parallel to the mean flow vorticity; second to distinguish between turbulence and secondary flow in the decomposition of the simulated flow field to enable the study of the mutual influence between the two.

The decomposition of the flow field is described in the next section. A brief overview of the numerical procedure is given in §3. The simulated flow fields are first considered as a unidirectional mean flow and deviations thereof (§4.1), and the latter are subsequently decomposed into a secondary flow field and turbulent fluctuations in §§4.2 and 4.3.

2. Flow field decomposition and governing equations

Consider plane Couette flow of an incompressible fluid as in figure 1, where the parallel walls move in opposite directions with velocity U_w in the x-direction so that the volume flow is zero; v' is the velocity in the wall-normal y-direction and w' the velocity in the spanwise z-direction. The channel is rotated about the z-axis with a constant angular velocity Ω. The rotation number is here defined as the ratio of twice the system angular velocity Ω to the shear rate of the laminar Couette flow, i.e. $Ro = 2\Omega h/U_w$, where h is the half-channel width. Note that the rotation number is the inverse of a Rossby number. Because the mean flow vorticity is $-\mathrm{d}U/\mathrm{d}y$, negative Ro means cyclonic background vorticity, while positive rotation numbers denote anticyclonic background vorticity. The bulk Reynolds number is defined as $Re = U_w h/\nu$ and the Reynolds number based on wall friction is $Re_\tau = u_\tau h/\nu$ where $u_\tau = (\tau_w/\rho)^{1/2}$ is the friction velocity, ρ is the density of the fluid and ν is the kinematic viscosity; τ_w denotes the magnitude of the wall shear stress.

The following notation will apply for the averaging and decomposition of the flow field. The average of a flow variable ϕ with respect to time and x-direction is denoted by $\overline{\phi}$. (The turbulence is assumed to be homogeneous in the x-direction and time.) Other spatial averages are denoted by $\langle\phi\rangle_\eta$ where the subscript denotes averaging along the η-axis. The instantaneous velocity u_i' can then be decomposed as

$$u_i' = U_i + \tilde{u}_i + u_i, \tag{2.1}$$

where

$$\left.\begin{aligned} U_i &= \langle \overline{u_i'} \rangle_z, \\ \tilde{u}_i &= \overline{u_i'} - U_i, \\ u_i &= u_i' - \overline{u_i'} = u_i' - (U_i + \tilde{u}_i). \end{aligned}\right\} \tag{2.2}$$

In unidirectional channel flow the mean or background flow is $\boldsymbol{U} = (U,0,0)$, whereas $\tilde{\boldsymbol{u}} = (\tilde{u},\tilde{v},\tilde{w})$ represents the secondary flow field, usually occurring as roll cells, or as disturbances to the background flow in the case of a laminar stability problem. $\boldsymbol{u} = (u,v,w)$ denotes turbulent fluctuations. This decomposition has been applied to curved channel flow by Moser & Moin (1987) and to non-rotating Couette flow by Lee & Kim (1991).

The streamwise momentum equation, (A 1) in the Appendix, averaged over (x,z)-planes and in time, can be integrated once to give

$$\nu \frac{\mathrm{d}U}{\mathrm{d}y} - \langle \tilde{u}\tilde{v} + \overline{uv} \rangle_z = \frac{\tau_w}{\rho}. \tag{2.3}$$

The transport equations for the energy of the secondary flow can be split into two: one equation for the energy of the cross-flow $\tilde{k}_c = \langle \frac{1}{2}(\tilde{u}_j \tilde{u}_j) \rangle_z$, $j = 2,3$, and another governing the streamwise component $\langle \frac{1}{2}\tilde{u}^2 \rangle_z$:

$$\begin{aligned} \frac{\mathrm{D}\tilde{k}_c}{\mathrm{D}t} = &-\frac{\mathrm{d}}{\mathrm{d}y}\left\langle \tilde{v}\overline{v^2} + \tilde{w}\overline{vw} \right\rangle_z - \frac{\mathrm{d}}{\mathrm{d}y}\left\langle \frac{1}{2}\left(\tilde{v}^3 + \tilde{v}\tilde{w}^2\right) \right\rangle_z - \frac{\mathrm{d}}{\mathrm{d}y}\left\langle \frac{\tilde{p}\tilde{v}}{\rho} \right\rangle_z \\ &+ \nu \frac{\mathrm{d}^2 \tilde{k}_c}{\mathrm{d}y^2} - \nu \left\langle \frac{\partial \tilde{v}}{\partial x_j}\frac{\partial \tilde{v}}{\partial x_j} + \frac{\partial \tilde{w}}{\partial x_j}\frac{\partial \tilde{w}}{\partial x_j} \right\rangle_z \\ &+ \left\langle \overline{v^2}\frac{\partial \tilde{v}}{\partial y} \right\rangle_z + \left\langle \overline{w^2}\frac{\partial \tilde{w}}{\partial z} \right\rangle_z + \left\langle \overline{vw}\left(\frac{\partial \tilde{v}}{\partial z} + \frac{\partial \tilde{w}}{\partial y}\right) \right\rangle_z - 2\Omega \langle \tilde{u}\tilde{v} \rangle_z, \end{aligned} \tag{2.4}$$

$$\begin{aligned} \frac{\mathrm{D}\langle \frac{1}{2}\tilde{u}^2 \rangle_z}{\mathrm{D}t} = &-\langle \tilde{u}\tilde{v} \rangle_z \frac{\mathrm{d}U}{\mathrm{d}y} - \frac{\mathrm{d}}{\mathrm{d}y}\langle \tilde{u}\overline{uv} \rangle_z - \frac{\mathrm{d}}{\mathrm{d}y}\left\langle \frac{1}{2}\tilde{u}^2\tilde{v} \right\rangle_z \\ &+ \nu \frac{\mathrm{d}^2 \langle \frac{1}{2}\tilde{u}^2 \rangle_z}{\mathrm{d}y^2} - \nu \left\langle \frac{\partial \tilde{u}}{\partial x_j}\frac{\partial \tilde{u}}{\partial x_j} \right\rangle_z + \left\langle \overline{uv}\frac{\partial \tilde{u}}{\partial y} \right\rangle_z + \left\langle \overline{uw}\frac{\partial \tilde{u}}{\partial z} \right\rangle_z + 2\Omega \langle \tilde{u}\tilde{v} \rangle_z. \end{aligned} \tag{2.5}$$

Here, weak system rotation corresponds to the situation where the channel mean value of the source term in (2.5) due to mean shear ($\langle -\langle \tilde{u}\tilde{v} \rangle_z \mathrm{d}U/\mathrm{d}y \rangle_y$) is significantly larger than the mean source/sink terms ($\langle \pm 2\Omega \langle \tilde{u}\tilde{v} \rangle_z \rangle_y$) in (2.4),(2.5) due to rotation. Around the centreline, the rotational and mean shear production can be of similar magnitude without conflicting with this argument. In this situation, there will be significant production of $\langle \frac{1}{2}\tilde{u}^2 \rangle_z$ and negligible production of $\tilde{k}_c$. Because of the two-dimensional nature of the secondary flow, the continuity equation can be separated into

$$\frac{\partial \tilde{u}}{\partial x} = 0 \quad \text{and} \quad \frac{\partial \tilde{v}}{\partial y} + \frac{\partial \tilde{w}}{\partial z} = 0. \tag{2.6}$$

This implies that there is no pressure–strain redistribution to take energy from $\langle \frac{1}{2}\tilde{u}^2 \rangle_z$ and feed it into $\tilde{k}_c$. The secondary flow is not redistributive in the same sense as the turbulence, which will strive towards isotropy through the action of the pressure–strain correlations. The consequence is that the secondary flow field will be highly anisotropic, i.e. approach the one-component limit due to the dominance of $\langle \frac{1}{2}\tilde{u}^2 \rangle_z$. The anisotropy of the secondary flow will be maintained unless there is significant

'indirect redistribution' through nonlinear interactions between secondary flow and turbulence. These interactions will be discussed in §4.3.

The above argument on the tendency to one-component secondary flow is valid in the present context because the terms due to rotation ($\pm 2\Omega\langle\tilde{u}\tilde{v}\rangle_z$) are small. When the background vorticity 2Ω approaches the mean vorticity at the centreline in the non-rotating case ($|-\mathrm{d}U/\mathrm{d}y| = 0.22$), another regime is entered. At these higher rotation rates, the rotational terms provide a significant energy transfer from $\langle\frac{1}{2}\tilde{u}^2\rangle_z$ to $\tilde{k}_c$, as will be discussed in Bech & Andersson (1996).

Consider the contraction of the transport equation for the (turbulent) Reynolds stresses $\overline{u_i u_j}$, (A 3) in the Appendix. By averaging in the z-direction we obtain the equation for the turbulent kinetic energy $k = \frac{1}{2}\langle\overline{u_j u_j}\rangle_z$:

$$\frac{\mathrm{D}k}{\mathrm{D}t} = -\langle\overline{uv}\rangle_z\frac{\mathrm{d}U}{\mathrm{d}y} - \frac{\mathrm{d}}{\mathrm{d}y}\left\langle\tfrac{1}{2}\overline{u_j u_j v} + \frac{\overline{pv}}{\rho}\right\rangle_z + \nu\frac{\mathrm{d}^2 k}{\mathrm{d}y^2} - \nu\overline{\frac{\partial u_j}{\partial x_k}\frac{\partial u_j}{\partial x_k}}$$

$$\underbrace{-\left\langle\overline{uv}\frac{\partial\tilde{u}}{\partial y}\right\rangle_z}_{+\tilde{P}_1} \quad \underbrace{-\left\langle\overline{uw}\frac{\partial\tilde{u}}{\partial z}\right\rangle_z}_{+\tilde{P}_2} \quad \underbrace{-\left\langle\overline{v^2}\frac{\partial\tilde{v}}{\partial y}\right\rangle_z}_{+\tilde{P}_3} \quad \underbrace{-\left\langle\overline{vw}\frac{\partial\tilde{v}}{\partial z}\right\rangle_z}_{+\tilde{P}_4} \quad \underbrace{-\left\langle\overline{vw}\frac{\partial\tilde{w}}{\partial y}\right\rangle_z}_{+\tilde{P}_5} \quad \underbrace{-\left\langle\overline{w^2}\frac{\partial\tilde{w}}{\partial z}\right\rangle_z}_{+\tilde{P}_6}. \tag{2.7}$$

Note that all the terms labelled as $\tilde{P}_n (n = 1, 6)$ occur with opposite signs in either (2.4) or (2.5) so that they represent nonlinear interactions between secondary flow and turbulence. The present investigation will try to shed some light on the character and magnitude of this energy exchange.

3. Numerical simulations

The direct numerical simulations (DNS) with system rotation performed here were continuations of the non-rotating turbulent plane Couette flow DNS reported by Bech *et al.* (1995). All simulations were run with the ECCLES code developed by Gavrilakis *et al.* (1986) at a Reynolds number $Re = 1300$. The code applies second-order-accurate central differences in space and explicit Adams–Bashforth discretization in time. The grid spacing was approximately 10 and 4 viscous, or wall, units ν/u_τ in the x- and z-directions, respectively, and the number of grid points was $256 \times 70 \times 256$. A non-uniform grid was applied in the y-direction. Because of the fine grid spacing applied here, the low-order numerical scheme should yield a reasonable resolution of the dynamically important scales of motion. Note that the numerical resolution is very similar to that applied in the accurate duct flow DNS by Gavrilakis (1992). Because the rotational effects on the *turbulent* motions were weak for $Ro = \pm 0.01$, the numerical resolution for the simulations at these rotation numbers was approximately the same as in the non-rotating case. The computational box was $10\pi h$ in the streamwise direction and $4\pi h$ in the spanwise direction, i.e. relatively large in terms of half-channel widths as compared to the simulation by Lee & Kim (1991), and somewhat larger, in terms of wall units, than the reference Poiseuille flow simulation by Kim, Moin & Moser (1987).

Effects of numerical resolution and size of computational domain on the numerical simulations of plane Couette flow at the present Re were investigated in our previous work (Bech & Andersson 1994). While Lee & Kim (1991) found roll cells in

simulations of the non-rotating flow, we concluded that this was one of at least two possible states in our simulations. Further, we found that the time scale was equally as important as the spatial scales for the existence of roll cells (in the non-rotating case), and that simulations of the Couette flow should preferably be run for a long time interval, in the same geometry, in order to eliminate influences from the (unphysical) initial flow field. In our previous work, we concluded that our final simulation of the non-rotating case, which did not contain roll cells, was the most consistent and reliable. This simulation, which was described and compared with experimental data by Bech *et al.* (1995), was used as the initial field for the simulations involving system rotation which are reported herein. Data from two cases, with $Ro = \pm 0.01$, will be presented in the next section together with data from the earlier simulation without rotation.

The present results are obtained by time-averaging statistically steady flow fields. The results from the simulation with $Ro = 0.01$ were time-averaged for a time of approximately $6h/u_\tau$ while the simulation with $Ro = -0.01$ was averaged for $2h/u_\tau$. This difference was motivated by the large-scale secondary vortices present for $Ro = 0.01$. Some of the results for the positive Ro (figures 10–13) will be based on averages over two flow fields sampled with a time interval of h/u_τ.

Prior to the DNS of the rotating turbulent plane Couette flow, linear stability calculations for the analogous laminar problem were performed. The present calculation was in agreement with the results of Lezius & Johnston (1976), and the critical curve in the (Re, Ro)-plane is described by $Re^2 Ro(1 - Ro) = 106.736$. The critical Reynolds number is $Re = 21$, at $Ro = 0.5$, which is also in agreement with the numerical investigation by Speziale & Wilson (1989). They studied a rotating laminar plane Couette flow with sidewalls, i.e. in a rectangular channel with one wall moving. One of our objectives in solving the laminar stability problem was to calculate the spanwise wavelength of the roll cells corresponding to the critical curve, in order to choose an appropriate computational domain for the DNS. The diameter of the roll cells will obviously be constrained by the height $2h$ of the computational domain. The actually chosen width $4\pi h$ then gives room for three pairs of counter-rotating cells. This corresponds to a spanwise wavelength of $4\pi h/3$, which is sufficiently close to the wavelength $4.04h$ that emerged from the linear stability analysis. Here, we draw parallels with the experimental results on Taylor–Couette flow by Smith & Townsend (1982), who observed that the wavelength differed little from the laminar to the turbulent case.

The linear stability analysis was repeated using the mean velocity profile from the DNS of non-rotating turbulent Couette flow instead of the linear velocity profile. Our objective in carrying out these calculations was to obtain an approximation for the critical value of the rotation number, i.e. the lowest value of Ro at which roll cells exist in the turbulent plane Couette flow at $Re = 1300$. The linearized equations result in an eigenvalue problem for the spanwise wavenumber of the disturbances with the wall-normal disturbance velocity $\tilde{v}$ as eigenfunction and Re and Ro as parameters. The eigenvalue problem was solved using four-step Runge–Kutta integration and a shooting technique. We actually solved the problem of neutral stability, and sought the lowest Ro, at $Re = 1300$, which gave a solution. This approach was somewhat related to that of Lezius & Johnston (1976), who introduced averaged eddy viscosities deduced from experimental data and constructed a two-layer flow model that was introduced in their stability calculations of the rotating Poiseuille flow. Their prediction of the critical value of the rotation number seemed to be reasonably successful.

4. Results

The critical Ro for onset of roll cell instabilities at $Re = 1300$ was predicted as 0.0002 by linear theory using the mean velocity profile from the non-rotating simulation. An additional DNS with $Ro = 0.001$, from which no quantitative results will be presented, was run with the non-rotating flow field as initial conditions. At time $\Omega t = 0.0065$, large-scale structures of approximately the same length scale as roll cells were observed in the secondary flow components. Structures with approximately half of this length scale were also seen. Later, at $\Omega t = 0.013$, the smaller structures were somewhat weakened, while the larger structures were more ordered and intense. At this low rotation rate, one would hardly expect strong instabilities, and the interpretation of the restricted amount of data was only qualitative. Of course, the time advancement should be of the order of one revolution in order to verify the onset of the roll cell instability, but unfortunately, such a simulation would have been very expensive with regard to computer time. However, the observations indicate that roll cells can occur at $Ro = 0.001$.

The concept of weak rotation needs some clarification in order to justify the title of the present paper. The vorticity ratio $S = -2\Omega/(\mathrm{d}U/\mathrm{d}y)$ is a useful parameter in order to evaluate the local influence of rotation. In the destabilized case, i.e. with $Ro = 0.01$, the local value of S varied from -0.02 near the wall to -0.27 at the centreline. One might therefore regard $Ro = 0.01$ as more than weak rotation. In the present work, however, we consider the direct effect of rotation upon the channel average of the production of the various components of the turbulent Reynolds stress tensor, whose transport equation is given by (A 3). It is therefore appropriate to use the y-averaged mean shear, so that $2\Omega/\langle \mathrm{d}U/\mathrm{d}y\rangle_y = -Ro$ becomes a suitable parameter. The significant value of S at the centreline at $Ro = 0.01$ was due to the mixing property of the roll cells, which reduced the non-dimensional mean shear $\mathrm{d}U/\mathrm{d}y$ from 0.22 in the non-rotating case, to 0.037 at $Ro = 0.01$. Because of the strong mixing, the central region cannot be isolated from the rest of the flow. At $Ro = 0.01$, the ratio of the channel averages of the rotational production (of $\langle \overline{u^2} \rangle_z$) to the mean shear production was 0.02. For the stabilizing case with $Ro = -0.01$, the maximum value of S was only 0.03. Based on these observations, the rotation number 0.01 was considered as low with regard to the influence of the Coriolis acceleration on turbulence intensity. However, the rotation rate was supercritical with respect to the roll cell instability, and therefore the destabilizing weak rotation had significant effects upon the flow field through the presence of the roll cells. As mentioned in §2, we will investigate higher rotation rates in a subsequent paper. In that work, we will show that strong rotation implies large rotational production, leading to a fundamental change of the turbulent Reynolds stress anisotropy.

Both stabilizing (negative, $Ro = -0.01$) and destabilizing (positive, $Ro = 0.01$) rotation will be considered in the first subsection, whereas the focus of interest in the second and third subsections will be the secondary flow and turbulence resulting from positive, or anticyclonic, rotation. The kinetic energy of the velocity fluctuations will be scaled with $u_{\tau,0}$ (from the simulation without rotation) and mean velocities with U_w. The y-axis is scaled by the half-channel width h, the walls being located at $y = \pm 1$. In some figures, only one half-channel is shown because the data from the two halves have been averaged.

4.1. *Spanwise-averaged statistics*

In this subsection deviations from the mean flow U are called fluctuations and no distinction is made between the secondary flow field $\tilde{\boldsymbol{u}}$ (which is non-zero only in

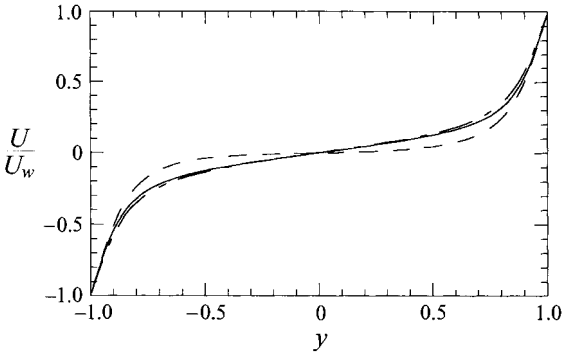

FIGURE 2. Mean velocity at different rotation rates. —, $Ro = 0$; - - -, $Ro = 0.01$; – - –, $Ro = -0.01$. Non-dimensionalized with U_w.

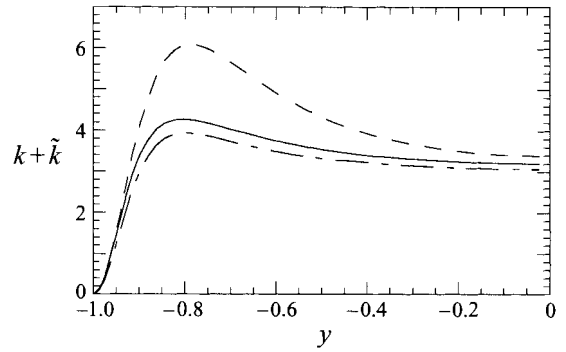

FIGURE 3. Kinetic energy of fluctuations. Legend as in figure 2. Non-dimensionalized with $u_{\tau,0}^2$.

Ro	Re_τ	$\langle k \rangle_y$	$\langle k + \tilde{k} \rangle_y$
0	82.2	3.30	3.30
−0.01	77.8	3.08	3.08
+0.01	84.7	2.70	4.05

TABLE 1. Gross flow parameters at different rotation numbers. $k = \frac{1}{2}\langle \overline{u_j u_j} \rangle_z$ and $\tilde{k} = \frac{1}{2}\langle \tilde{u}_j \tilde{u}_j \rangle_z$, $j = 1, 2, 3$. Note that $u_{\tau,0}$ was used for non-dimensionalizing and that the values for Re_τ can be used to rescale. In the stable cases ($Ro = 0$ and -0.01), $\tilde{k} \equiv 0$ because the two-component decomposition was applied.

the case $Ro = 0.01$) and the turbulence $\boldsymbol{u}$. In figure 2, the mean velocity profile of the non-rotating Couette flow is compared with the profiles resulting from imposing positive and negative rotation. The effect of negative system rotation ($Ro = -0.01$) was to damp the velocity fluctuations slightly as can be readily seen in figure 3. This is consistent with a small reduction of the Reynolds number Re_τ, see table 1. The decrease of wall shear stress was counter-balanced by a slightly increased mean shear in the central region. The volume-averaged kinetic energy $\langle k \rangle_y$ of the fluctuations was damped by 7%.

Positive rotation led to substantial increase in $\langle k + \tilde{k} \rangle_y$ (figure 3) and the gain in volume-averaged energy of fluctuations was 23% (in dimensional quantities). The

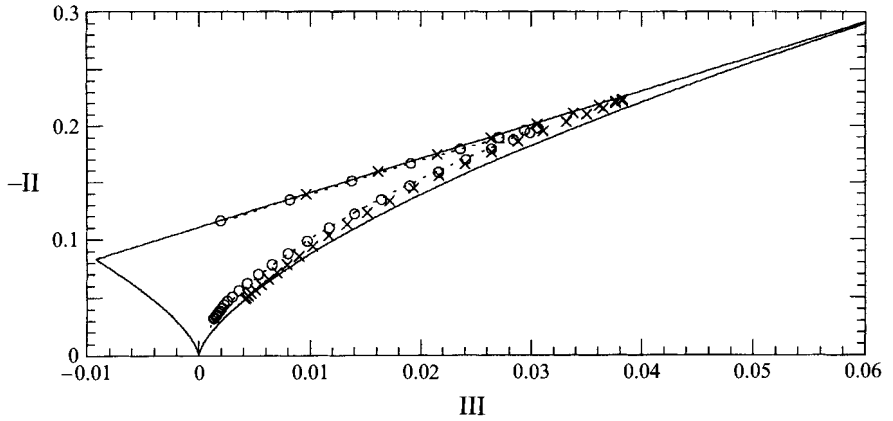

FIGURE 4. Anisotropy invariant map (AIM) for total fluctuations $(\tilde{u}_i + u_i)$. - - -, $Ro = 0$; ×, $Ro = 0.01$; ○, $Ro = -0.01$.

mean velocity in figure 2 exhibits a large flat region resulting from the enhanced mixing in the wall-normal y-direction for $Ro = 0.01$. The wall region with high mean shear was enlarged, and it is seen from figure 3 that the increase in kinetic energy was most significant in the peak region. The peak was also moved further away from the wall.

Following Lumley (1978), we calculate the invariants

$$\mathrm{II} = \tfrac{1}{2}(a_{ii}a_{jj} - a_{ii}^2), \quad \mathrm{III} = \tfrac{1}{3!}(a_{ii}a_{jj}a_{kk} - 3a_{ii}a_{jj}^2 + 2a_{ii}^3) \tag{4.1}$$

where a_{ij} is the anisotropy tensor of the second moments of the total fluctuations $u_i + \tilde{u}_i$, i.e.

$$a_{ij} = \frac{\langle \overline{u_i u_j} \rangle_z + \langle \tilde{u}_i \tilde{u}_j \rangle_z}{2(k + \tilde{k})} - \frac{\delta_{ij}}{3}. \tag{4.2}$$

Note that a_{ii}^2 and a_{ii}^3 denote the traces of $a_{ij}^2 = a_{ik}a_{kj}$ and $a_{ij}^3 = a_{ik}a_{kl}a_{lj}$, respectively. The anisotropy invariant map (AIM) is shown in figure 4 for all three cases. The data are contained in an area spanned by lines corresponding to axisymmetric contraction, axisymmetric expansion and the two-component limit (the upper straight line). Each data point in the AIM corresponds to distinct separations from the wall. The points that touch the two-component limit correspond to positions close to the walls ($y = \pm 1$), where wall-normal velocity fluctuations are damped, while the fluctuations near the channel centre ($y = 0$) were closest to isotropy, i.e. to the origin in the AIM.

Negative rotation did not influence the anisotropy to any discernible degree. By rotating the system in the positive sense, a marked change in the invariants was recognized around the point where both −II and III attained their maxima. This corresponds to the region of maximum kinetic energy in physical space (see figure 3). The effect of positive rotation was to make one component of the fluctuations, i.e. the streamwise, significantly more intense than the other two, so that the points were shifted towards the upper right corner in the AIM.

4.2. *Decomposition into secondary flow and turbulence*

Because of the close similarities between the non-rotating case (which has been investigated before) and the case with $Ro = -0.01$, we will concentrate on the case with positive rotation and decompose the flow field so that the turbulence fluctuations (u_i) are separated from the secondary flow ($\tilde{u}_i$). By subtraction of the

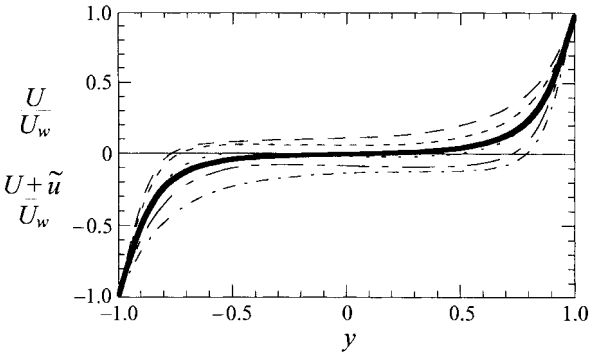

FIGURE 5. Sum of mean and secondary velocity ($U + \tilde{u}$) at five different z positions, $Ro = 0.01$. Bold line: U. Non-dimensionalized with U_w.

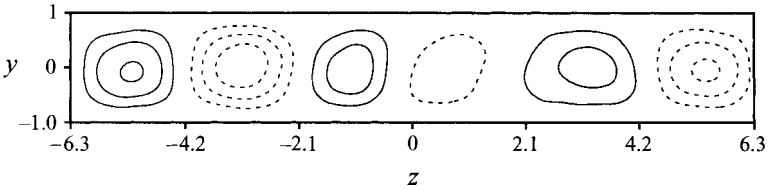

FIGURE 6. Cross-flow stream function non-dimensionalized with $U_w h$, $Ro = 0.01$. Contour increment = 0.01. Dashed lines: negative.

turbulent fluctuations, the remaining streamwise velocity $U + \tilde{u}$ becomes a function of y and z, see figure 5. The velocity profiles at some different spanwise positions show how the secondary flow modulates the streamwise velocity component. High shear near one wall coincided with low shear near the other wall because of the large-scale mixing induced by the roll cells. The wavelength of the secondary velocity was forced by the width of the computational box so that it was $4\pi/3 \simeq 4.19$.

The slightly irregular secondary flow pattern can be recognized in figure 6. Since the flow field had been averaged in time and the x-direction, however, the roll cells were considered as rather persistent, and the assumption that there existed a secondary flow independent of x and t was justified. The secondary motion in the (y, z)-plane will be referred to as cross-flow to distinguish it from the streamwise component of the secondary flow.

In figure 7, the normal stresses for the case $Ro = 0.01$ are visualized. The secondary component $\langle \tilde{u}^2 \rangle_z$ was of the same magnitude as the turbulent stress $\langle \overline{u^2} \rangle_z$, while the secondary cross-flow was relatively weak. It is seen that $\langle \tilde{v}^2 \rangle_z$ attains its maximum at the centreline while $\langle \tilde{w}^2 \rangle_z$ exhibits a maximum around $y = -0.7$, i.e. in accordance with roll cells filling most of the cross-section. In this case, the volume-averaged secondary energy $\langle \tilde{k} \rangle_y$ amounted to 33% of the total kinetic energy $\langle k + \tilde{k} \rangle_y$ while the turbulent kinetic energy $\langle k \rangle_y$ was smaller than in the non-rotating case by 18% (see table 1). The intensity of the cross-flow, visualized in figure 6, was relatively low. However, the weak mixing in the cross-sectional plane associated with the cross-flow was sufficient to influence the streamwise velocity profile significantly and to generate a substantial spanwise variation of the secondary streamwise velocity. The cross-flow was one order of magnitude less intense than the streamwise secondary velocity, so that the secondary flow exhibited strong anisotropy, as can be seen from the AIM in figure 8, where the anisotropies of the turbulence and secondary flow are treated separately. While the turbulence anisotropy invariants were practically the same as in

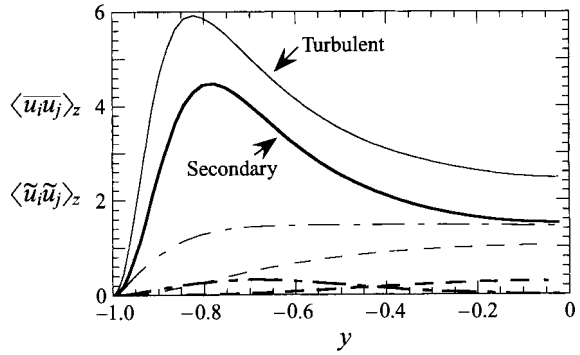

FIGURE 7. Turbulent (thin lines) and secondary (bold lines) normal stresses for the case $Ro = 0.01$. —, $\langle \overline{u^2} \rangle_z$ and $\langle \tilde{u}^2 \rangle_z$; – – –, $\langle \overline{v^2} \rangle_z$ and $\langle \tilde{v}^2 \rangle_z$; — – —, $\langle \overline{w^2} \rangle_z$ and $\langle \tilde{w}^2 \rangle_z$. Non-dimensionalized with $u_{\tau,0}^2$.

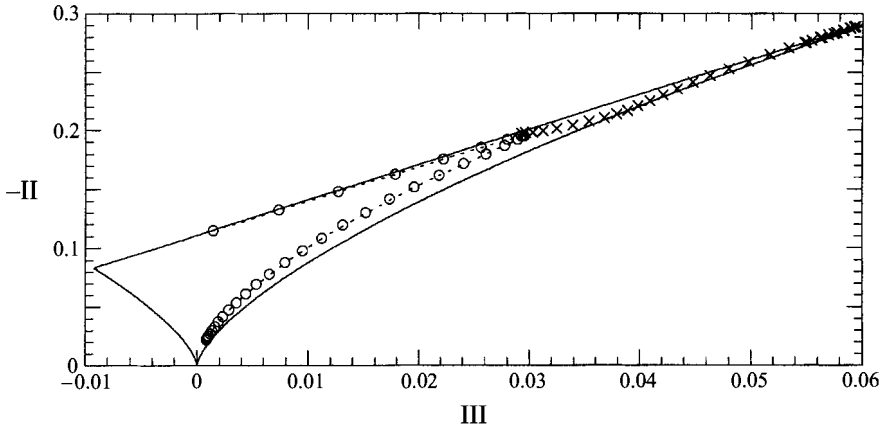

FIGURE 8. AIM for turbulence and secondary flow.
- - -, $Ro = 0$; ×, $Ro = 0.01$, secondary; ○, $Ro = 0.01$, turbulent.

the non-rotating case, the secondary flow approached the one-component limit due to the dominance of $\langle \frac{1}{2}\tilde{u}^2 \rangle_z$.

The variation of the shear stresses $-\langle \overline{uv} \rangle_z$ and $-\langle \tilde{u}\tilde{v} \rangle_z$ in the case with $Ro = 0.01$ is visualized in figure 9. From (2.3), it is known that the sum of the viscous, turbulent and secondary shear stresses is constant and equal to the wall shear stress. Because of this, the turbulent shear stresses in figure 9 exhibit their maxima at the centreline. The difference between the non-rotating and the stabilized case is seen to be rather small and in accordance with the slightly reduced turbulent kinetic energy for $Ro = -0.01$ which was observed in figure 3. For these two cases, the sum $-(\langle \overline{uv} \rangle_z + \langle \tilde{u}\tilde{v} \rangle_z)$ is plotted†. In the destabilized case, however, the two components are plotted separately. The most important inference from this figure is that the turbulent and secondary shear stresses are of approximately the same magnitude at $Ro = 0.01$. The secondary component also exhibited a maximum away from the centreline and was more than twice as large as the turbulent shear stress close to the walls.

The spanwise spacing between low-speed streaks in near-wall flows has been measured from both physical and numerical experiments in the non-rotating case,

† In the cases where no roll cells were observed, there was a small non-zero contribution to the secondary quantities due to the finite extent of the computational box and the finite sampling time, cf. the discussion at the beginning of §5.

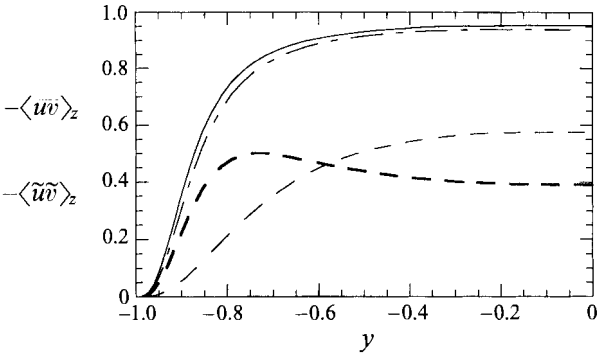

FIGURE 9. Shear stresses at three different rotation rates: —, $Ro = 0$; - - -, $Ro = 0.01$; – – –, $Ro = -0.01$. For the case $Ro = 0.01$, both turbulent shear stress $-\langle\overline{u}\overline{v}\rangle_z$ (thin line) and secondary shear stress $-\langle\tilde{u}\tilde{v}\rangle_z$ (bold line) are shown. For the other rotation rates, only the total shear stresses are shown. Non-dimensionalized with u_τ^2.

and there seems to be general agreement that the spacing λ^+, in wall units, should be close to 100. Kristoffersen & Andersson (1993) calculated λ^+ on the destabilized side of their simulated rotating Poiseuille flow, and found a significant decrease, except in the case with rotation number 0.01, i.e. sub-critical with respect to roll cell instabilities. In the present, destabilized case with $Ro = 0.01$, an *increase* of around 10% was observed in λ^+, i.e. the opposite of what one could expect from observations of rotating Poiseuille flow. Here, λ was calculated from the two-point correlation $R_{uu}(r_z)$ displayed in figure 10. The half-streak spacing was defined as the distance to the first minimum in the correlation curve, and made non-dimensional with ν/u_τ. Because u_τ is larger in the destabilized case than for $Ro = 0$, the actual increase in λ is somewhat smaller than 10%. There were some uncertainties in the present results due to the fact that λ was not a smooth function of the distance to the nearest wall. We used an average in the interval $2 < y^+ < 10$, where $y^+ = (1 - |y|)Re_\tau$, but the variation of λ in this interval was of the same order as the variation between the different rotation rates. Hence, our results on the streak spacing must be considered as somewhat uncertain. λ was only about 30% of the spanwise wavelength of the roll cells, so that the slight increase in λ was not some kind of resonance phenomenon. In figure 10, two correlation curves are given in the destabilized case: a thin curve for the turbulent component and a thick one for the sum of the secondary and turbulent components of the streamwise velocity. In the latter case, the spanwise variation of the secondary flow with its wavelength slightly above four is dominant. In the stabilized case with $Ro = -0.01$, λ^+ showed a slight increase (around 5%) compared to the non-rotating case.

A more quantitative measure of the activity of turbulence-generating events can be found in figure 11, where the frequency of occurrence of VISA events is plotted versus the variable averaging interval. A VISA (Variable Interval Space Averaging) event occurs when the local variance of u over an interval of length L^+ exceeds the overall variance. Such events take the shape of curved internal shear layers and are assumed to be important for the transfer of energy from mean flow to turbulence. In figure 11, results for $Ro = \pm 0.01$ have been compared with both experiments and simulation data at $Ro = 0$, using Taylor's hypothesis and the propagation velocity of the VISA events at $Ro = 0$ to compare these results, see Bech *et al.* (1995) for details. The frequency of turbulence-generating events was reduced due to system rotation in accordance with the reduction of turbulent kinetic energy $\langle k\rangle_y$ shown in table 1.

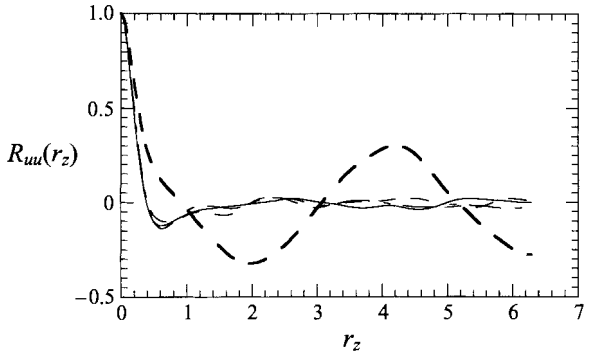

FIGURE 10. Two-point correlations for the velocity component u in the lateral direction z for three different Ro. Legend as in figure 9. For $Ro = 0.01$, the bold line shows the correlation for the sum $u + \tilde{u}$.

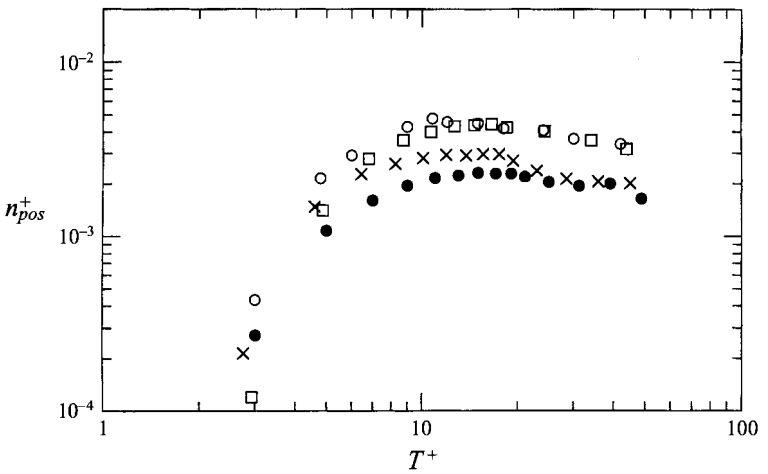

FIGURE 11. Frequency of occurrence of positive VISA events and VITA events. Inner scaling. ○, Experiments; □, DNS; data for $Ro = 0$, see Bech *et al.* (1995); •, $Ro = +0.01$; ×, $Ro = -0.01$. The results for $Ro = -0.01$ are based on one flow field, i.e. only spatial averaging.

The most significant reduction occurred in the case where secondary roll cells were a predominant feature of the flow, i.e. for $Ro = 0.01$.

4.3. *Transfer of energy between secondary flow and turbulence*

The possible exchange of energy between the turbulence and the secondary flow will now be investigated, and we therefore consider the case $Ro = 0.01$ only. First, note that the channel average of the sink/source terms $\pm 2\Omega\langle\tilde{u}\tilde{v}\rangle_z$ due to rotation were only about 2% of the source term in (2.5) due to mean shear, $\tilde{P} = -\langle\tilde{u}\tilde{v}\rangle_z \mathrm{d}U/\mathrm{d}y$. Thus, even if the magnitude of the local vorticity ratio $S = -2\Omega/(\mathrm{d}U/\mathrm{d}y)$ became as high as 0.27 at the centreline, the direct effect of system rotation on turbulence was weak, as discussed in the beginning of this section. It is therefore of interest to consider other source/sink terms in the equations for the components of the Reynolds stress tensor. In this subsection, our focus will be on the role of the secondary production terms $\tilde{P}_n$ together with the conventional production term $P = -\langle\overline{uv}\rangle_z \mathrm{d}U/\mathrm{d}y$, see (2.7), and the secondary production $\tilde{P}$ of (2.5).

From the turbulent and secondary Reynolds shear stresses in figure 9, it can be

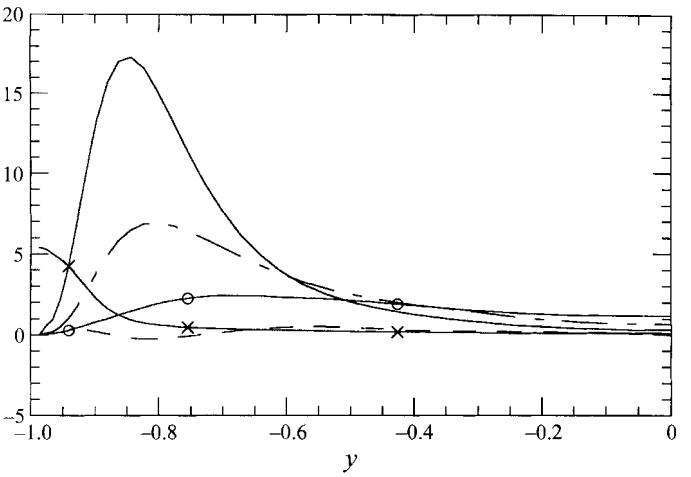

FIGURE 12. Various production and dissipation-rate terms. All terms are shown positive for comparative purposes. —, P; - - -, $\tilde{P}$; - · -, $\tilde{P}_1$; ○, $\tilde{P}_2$; ×, $\tilde{\varepsilon}_{11} = \nu\langle\partial\tilde{u}/\partial x_j \partial\tilde{u}/\partial x_j\rangle_z$. Non-dimensionalized with $u_{\tau,0}^3/h$.

deduced that P and $\tilde{P}$ were of approximately the same magnitude. The actual value of the ratio $\langle\tilde{P}\rangle_y/\langle P\rangle_y$ was 0.52. This is in accordance with the ratio between $\langle\tilde{u}^2\rangle_z$ and $\langle\overline{u^2}\rangle_z$ (see figure 7). Because there was no inter-component energy transfer between $\langle\frac{1}{2}\tilde{u}^2\rangle_z$ and $\tilde{k}_c$, except the weak rotational redistribution through $\pm 2\Omega\langle\tilde{u}\tilde{v}\rangle_z$, the energy in the $\langle\frac{1}{2}\tilde{u}^2\rangle_z$-component must either be dissipated in the secondary flow or transferred to the turbulence through the terms $\tilde{P}_1$ and $\tilde{P}_2$. Figure 12 shows some of the production terms. The viscous dissipation-rate term of (2.5) is also shown. The main sink term for $\langle\frac{1}{2}\tilde{u}^2\rangle_z$ was $-\tilde{P}_2$. The ratio $\langle\tilde{P}_2\rangle_y/\langle\tilde{P}\rangle_y$ was 0.49, i.e. approximately half the energy transfer from the mean flow to the secondary flow was passed on to the turbulence, while about 40% was dissipated in the secondary motion in the vicinity of the walls. The net effect of $-\tilde{P}_1$ was one order of magnitude smaller than that of $-\tilde{P}_2$.

From the point of view of (2.7), the two most important source terms for the turbulence were the primary production P and the secondary production $\tilde{P}_2$. By y-averaging, it was found that the latter was about 25% of the former. $\tilde{P}_2$ was the largest production term in the central region of the flow. Note that the primary production was significantly reduced by destabilizing rotation because the mean shear was reduced. The damping of turbulence in the central region can then be considered as a result of the flattening of the mean velocity profile, which again was a result of the cross-flow mixing. However, the secondary streamwise motion, which was also induced by the cross-flow, prevented annihilation of the turbulence in the central region by transferring energy through $\tilde{P}_2$.

As a consequence of the weak cross-flow and therefore the secondary shear rates, the energy transfer between $\tilde{k}_c$ and k was small. The terms $-\tilde{P}_n$ $(n = 3, 6)$ are displayed in figure 13(a). The magnitudes were only a few percent of $\tilde{P}_2$. In order to deduce the net energy transfer to the cross-flow, the sum $\sum_{n=3}^{6} -\tilde{P}_n$ was plotted together with the rotational production term of (2.4) in figure 13(b). The energy transfer between cross-flow and turbulence changed sign about halfway between the wall and the centreline, while the rotational term acted as a source all across the channel. This implies that the turbulence supplied energy to the cross-flow in the near-wall region. In this part of the flow, the rotational term $-2\Omega\langle\tilde{u}\tilde{v}\rangle_z$ was weak and the

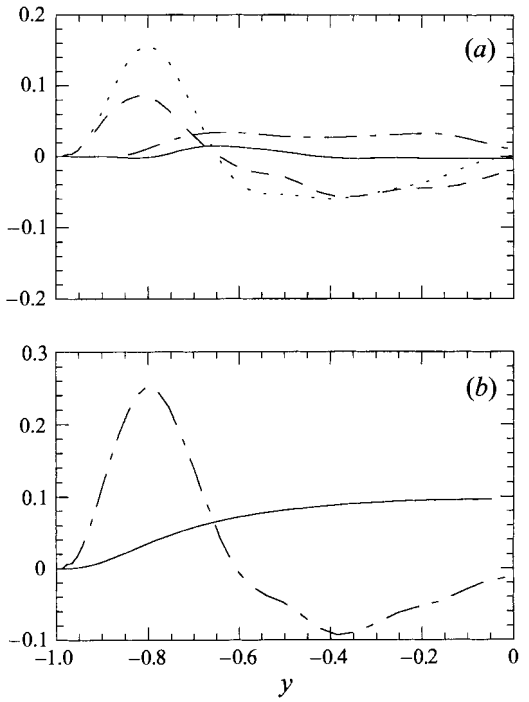

FIGURE 13. (*a*) Secondary production terms. —, $-\tilde{P}_3$; - - -, $-\tilde{P}_4$; - - -, $-\tilde{P}_5$; · · ·, $-\tilde{P}_6$. (*b*) Rotational and secondary production terms of (2.4). —, $-2\Omega\langle\tilde{u}\tilde{v}\rangle_z$; - - -, $\sum_{n=3}^{6} -\tilde{P}_n$. Same scaling as in figure 12.

viscous stresses damped the secondary motion. In addition, the primary turbulence production reached its peak value here. In the central region of the flow, the 'cascade' behaviour was retained, i.e. energy from the cross-flow was fed into the turbulence. By averaging in the y-direction, however, a slight transfer from turbulence to cross-flow was observed, and this transfer was larger than the rotational effect.

5. Discussion and conclusions

First, a remark should be made about the decomposition of the flow field. The filter applied to separate the velocity (and pressure) fluctuations into a secondary component and turbulence was somewhat influenced by the geometry of the computational domain. Because the streamwise extent of the computational domain was finite, i.e. about 2500 wall units, the secondary flow inevitably contained some small contributions from the near-wall low-speed streaks with a typical length scale of 1000 wall units. In Couette flow, the elongated regions of high and low streamwise momentum observed in the central region of the non-rotating flow, i.e. the largest scales of turbulence, were even more likely to contribute to the secondary component. In the present non-rotating case, roughly 8% of the turbulent kinetic energy was filtered out as secondary flow. Note, however, that in the presentation of the results, this 8% was counted as turbulence, and not as secondary flow. In the results given here, only the destabilized flow field ($Ro = 0.01$), where actual roll cells were observed, was subject to the three-component filter. In that case, it therefore seems reasonable to estimate that the contribution to the kinetic energy from the secondary flow was between 20% and 30%, and not exactly 33% as stated in the previous section. The important conclusion of this paper, namely that the turbulence was damped in the

destabilized case, is still significant. It should also be stressed that the total kinetic energy, as given in table 1, is independent of the decomposition applied.

The present results for weakly rotating plane Couette flow showed that the turbulence was damped regardless of the sense of rotation. Negative, or cyclonic, rotation, which is stabilizing in the case of laminar flow, was associated with a modest damping of the turbulent fluctuations. The effect of weak cyclonic rotation ($Ro = -0.01$) was considered as a perturbation of the mean statistics similar to a slight decrease in Reynolds number. A slight decrease in the turbulence intensity was observed. Following the line of argument presented by Kristoffersen & Andersson (1993), we consider the 11-, 22- and 12-components of (A 3). With weak stabilizing rotation, the vorticity ratio S is small everywhere in the channel, and the mean shear production terms are substantially larger than the rotational production terms. Thus the rotational generation term $-2\Omega\langle\overline{uv}\rangle_z$ is only important for the 22-component, where no mean shear generation is present, and it is thus seen that negative rotation tends to damp $\langle\overline{v^2}\rangle_z$. This results in less mean shear generation of $-\langle\overline{uv}\rangle_z$ through the term $\langle\overline{v^2}\rangle_z \mathrm{d}U/\mathrm{d}y$. To close the circle of arguments, the mean shear production of $\langle\overline{u^2}\rangle_z$ decreases when $-\langle\overline{uv}\rangle_z$ is damped, thus resulting in lower turbulent kinetic energy. Owing to the increased complexity caused by the presence of roll cells in the destabilized case, this type of argument is not applicable in the case with $Ro = 0.01$, which will be discussed below.

Positive, or anticyclonic, rotation caused counter-rotating streamwise-oriented roll cells to develop analogous to what is found in the laminar case. The rather steady and persistent secondary flow caused strong mixing in the wall-normal direction. Owing to this efficient mixing, the mean velocity profile exhibited a large region of low shear around the centreline. The secondary cross-flow $(\tilde{v}, \tilde{w})$ was rather weak while the streamwise component of the secondary flow was about as energetic as the turbulence fluctuations. The turbulent Couette flow seems to be more unstable with respect to roll cell instabilities than the turbulent Poiseuille flow. The two flows respond differently to system rotation due to the symmetry/antisymmetry of their mean velocity profiles. Kristoffersen & Andersson (1993) observed that $\langle\overline{u^2} + \tilde{u}^2\rangle_z$ increased by almost 50% when the rotation number was increased from 0.01 to 0.10. This substantial growth was probably mainly due to the onset of roll cell instabilities. At Reynolds number $Re = 2900$ the critical rotation number was in the interval $(0.01, 0.05)$. Lezius & Johnston (1976) calculated a critical value of 0.02, also for rotating Poiseuille flow, by using linear theory and empirical correlations, while Johnston *et al.* (1972) observed that the critical rotation number was less than 0.04.

No direct measure of the critical Ro was obtainable from the present Couette flow simulations. However, linear analysis using the mean velocity profile from the non-rotating simulation gave a stability limit for onset of roll cell instabilities. The critical rotation number was estimated as $Ro = 0.0002$ at the present Re. This was consistent with DNS that indicated that roll cells could exist at Ro below 0.001. But because the large-scale velocity fluctuations in non-rotating Couette flow bear some resemblance to roll cells, this observation is not conclusive. At low rotation rates, the turbulent fluctuations will be more intense than eventual roll cells, and the linearization applied in the stability problem is indeed very approximate. However, we expect the critical Ro to be lower in the Couette flow than in the Poiseuille flow owing to the antisymmetric velocity profile of the former, but this point should be subject to further investigations. In fact, roll cell instabilities have also been observed in DNS of non-rotating plane Couette flow, see Lee & Kim (1991), Kristoffersen, Bech & Andersson (1993) and Papavassiliou (1993).

Another difference between Poiseuille and Couette flows was associated with the topology of the roll cells. In rotating or slightly curved Poiseuille flow, as simulated by Kristoffersen & Andersson (1993) and Moser & Moin (1987), respectively, well-defined *pairs* of counter-rotating vortices of the Görtler type were observed. These pairs were asymmetric with respect to the centreline and caused substantial and localized momentum transport away from the pressure side and a more diffuse flow from the suction side back to the pressure side. In figure 6, the roll cells are seen to be symmetric about $y = 0$ because both sides were either pressure or suction sides in the rotating Couette flow. Obviously, the antisymmetry of the mean velocity profile makes the symmetry of the roll cell pattern in rotating Couette flow qualitatively different from that observed in pressure-driven flow. In fact, complete arbitrariness exists concerning with which of its nearest neighbours a particular cell forms a pair. We will return to the study of the roll cells in a subsequent work, where flow structures and vorticity will be examined at higher rotation rates.

The mean flow supplied energy to the secondary flow and the turbulence, the ratio of these energy transfers being $\langle \tilde{u}\tilde{v} \rangle_z / \langle \overline{uv} \rangle_z$. With destabilizing rotation, the energy loss from the mean flow, as represented by the last term in (A 2), decreased by about 10% as compared to the non-rotating case. This decrease took place in the region around the centreline because the mean shear rate in this area was reduced due to the mixing induced by the roll cells, while there was an increase in the mean shear close to the walls. The substantial transfer of energy to the secondary flow therefore implied a reduced transfer to the turbulence as compared to the non-rotating case in which $\langle \tilde{u}\tilde{v} \rangle_z$ was practically absent. As has been discussed previously, the wall friction increased in the destabilized case. Because this implied an increase in the work done by the solid walls on the fluid, and at the same time, the energy transfer to the fluctuating field was reduced, the dissipation rate of the mean field, i.e. $\nu(\mathrm{d}U/\mathrm{d}y)^2$ in (A 2), exhibited a significant increase.

In summary, the energy transfer between the flow components can be described as follows. The energy transfer from the mean flow to the secondary flow was directed into the $\langle \frac{1}{2}\tilde{u}^2 \rangle_z$ component. The exchange between $\tilde{k}_c$ and $\langle \frac{1}{2}\tilde{u}^2 \rangle_z$ due to rotational source and sink terms was marginal, i.e. about 4% of the secondary production $\tilde{P}$. Because the secondary flow is independent of the streamwise position, no pressure–strain redistribution is present in the transport equations (2.4) and (2.5). The result is a substantial anisotropy, towards one-componentality, of the secondary flow. The anisotropy was somewhat reduced by a significant energy transfer from $\langle \frac{1}{2}\tilde{u}^2 \rangle_z$ to the turbulent kinetic energy k through the term $\tilde{P}_2$ which represents a correlation between the wall-normal secondary vorticity $\tilde{\omega}_y = \partial\tilde{u}/\partial z$ and the 'cross-flow' Reynolds shear-stress $-\overline{uw}$ (note that $\langle -\overline{uw} \rangle_z = 0$). This transfer was approximately 25% of the primary turbulence production P. There was modest 'backscattering' of energy from turbulence to cross-flow due to the terms $\sum_{n=3}^{6} \tilde{P}_n$. The primary turbulence production was significantly reduced due to the onset of the roll cell instability.

The resulting damping of turbulence in the case of destabilizing rotation is somewhat surprising. Johnston *et al.* (1972) found a reduction of the burst rate on the stabilized side of rotating Poiseuille flow and concluded that no evidence of increase in the burst activity was observed on the destabilized side, unlike what they expected to find. (Note that the bursting processes are solely responsible for production of turbulent kinetic energy and are not connected to secondary flow, see for example Kim, Kline & Reynolds 1971.) The present results show that the burst rate was somewhat reduced with stabilizing rotation, probably because the stabilizing effect

acts on both mean flow and turbulence in accordance with former observations. The streak spacing was somewhat increased for $Ro = -0.01$, but only in non-dimensional quantities. There was no increase of the dimensional streak spacing, and the uncertainties in the results prevent any firm conclusions being drawn. The results for the frequency of VISA events were, however, more significant. The reduction in the burst frequency was accompanied by decreasing turbulent kinetic energy and wall shear stress in the stabilizing case. However, the reduction in the burst rate was even more pronounced with destabilizing rotation. This reduction cannot be ascribed directly to the Coriolis effect on turbulence, but must be caused by the secondary flow, as proposed by Johnston *et al.* In the case of Couette flow, the production of turbulence is reduced by the presence of a significant secondary flow component, so that a smaller amount of the kinetic energy in the near-wall region is associated with bursting and a greater fraction of energy is associated with a large-scale spanwise variation of the streamwise velocity set up by the roll cells. Note also that the bursting frequency decreased while the wall friction increased at $Ro = 0.01$. This was because the roll cells made a significant contribution to the wall shear stress, which is quite interesting from a turbulence control viewpoint. It is possible that the two-dimensionality of the roll cells suppresses the development of inclined internal shear layers which are typical of the VISA events detected here. Johnston *et al.* suggested that roll cells inhibit the streak bursting process, i.e. that the low-speed streaks were convected away from the high-shear region before they burst. This is not fully in accordance with the present results because the streak spacing was observed to increase, leading to a reduced streak density. Thus, the reduced burst frequency was not necessarily a result of the influence of the roll cells on the bursting process itself, but rather on the formation of streaks. One may, for instance, anticipate that the spanwise regularity and large length scale imposed on the near-wall turbulence by the roll cells suppress the formation of more or less randomly occurring streaks with smaller length scales. In this way, formation of roll cells is a somewhat peculiar turbulence control mechanism that increases both mixing and wall shear stress.

While the secondary flow was highly anisotropic, the anisotropy of the turbulence was essentially the same in all three cases. Even though the frequency of turbulence-generating events was reduced, the structure of the turbulence was practically unaffected by the secondary flow. The concept of stabilizing or destabilizing system rotation has been shown to be rather ambiguous since in the case in which the background flow was destabilized, the turbulence was damped.

This work has received support from The Research Council of Norway (Programme for Supercomputing) through a grant of computing time. Professor Henrik Alfredsson, Stockholm, made an instructive comment on the VISA events. The referees are acknowledged for valuable comments and suggestions for improvements.

Appendix. Transport equations

The momentum equation for an incompressible fluid in a coordinate system with z-wise rotation can be written

$$\frac{\mathrm{D}u_i}{\mathrm{D}t} = -\frac{1}{\rho}\frac{\partial p}{\partial x_i} + \nu\frac{\partial^2 u_i}{\partial x_j \partial x_j} - 2\Omega\epsilon_{i3k}u_k. \tag{A 1}$$

The 'centrifugal' acceleration has been included in the pressure term, see for example

Greenspan (1968). The transport equation of the mean flow kinetic energy $K = \frac{1}{2}U^2$ is

$$\frac{DK}{Dt} = \nu\frac{d^2K}{dy^2} - \nu\left(\frac{dU}{dy}\right)^2 - \frac{d}{dy}\left(U\langle\overline{uv} + \tilde{u}\tilde{v}\rangle_z\right) + \langle\overline{uv} + \tilde{u}\tilde{v}\rangle_z\frac{dU}{dy}. \tag{A 2}$$

The equation for the (turbulent) Reynolds stresses, averaged in the x-direction and time t, can be written

$$\begin{aligned}\frac{D\overline{u_iu_j}}{Dt} = &-\overline{u_iu_k}\frac{\partial U_j}{\partial x_k} - \overline{u_ju_k}\frac{\partial U_i}{\partial x_k} - \overline{u_iu_k}\frac{\partial\tilde{u}_j}{\partial x_k} - \overline{u_ju_k}\frac{\partial\tilde{u}_i}{\partial x_k}\\ &-\frac{\partial}{\partial x_k}\left[\overline{u_iu_ju_k} + \frac{\overline{pu_i}}{\rho}\delta_{jk} + \frac{\overline{pu_j}}{\rho}\delta_{ik}\right] + \frac{1}{\rho}\overline{p\left(\frac{\partial u_i}{\partial x_j} + \frac{\partial u_j}{\partial x_i}\right)}\\ &+\nu\frac{\partial^2\overline{u_iu_j}}{\partial x_k\partial x_k} - 2\nu\overline{\frac{\partial u_i}{\partial x_k}\frac{\partial u_j}{\partial x_k}} - 2\Omega\overline{u_m\left(\epsilon_{i3m}u_j + \epsilon_{j3m}u_i\right)}.\end{aligned} \tag{A 3}$$

REFERENCES

ALFREDSSON, P. H. & PERSSON, H. 1989 Instabilities in channel flow with system rotation. *J. Fluid Mech.* **202**, 543.

BECH, K. H. & ANDERSSON, H. I. 1994 Very large scale structures in DNS. In *Direct and Large-Eddy Simulation I* (ed. P.R. Voke, L. Kleiser & J.-P. Chollet), p. 13. Kluwer.

BECH, K. H. & ANDERSSON, H. I. 1996 Growth and decay of longitudinal roll cells in rotating turbulent plane Couette flow. In *Proc. 6th European Turbulence Conference, Lausanne* (to be published by Kluwer).

BECH, K. H., TILLMARK, N., ALFREDSSON, P. H. & ANDERSSON, H. I. 1995 An investigation of turbulent plane Couette flow at low Reynolds numbers. *J. Fluid Mech.* **286**, 291.

BIDOKHTI, A. A. & TRITTON, D. J. 1992 The structure of a turbulent free shear layer in a rotating fluid. *J. Fluid Mech.* **241**, 469.

BRADSHAW, P. 1987 Turbulent secondary flows. *Ann. Rev. Fluid Mech.* **19**, 53.

CAMBON, C., BENOIT, J.-P., SHAO, L. & JACQUIN, L. 1994 Stability analysis and large-eddy simulation of rotating turbulence with organized eddies. *J. Fluid Mech.* **278**, 175.

GAVRILAKIS, S. 1992 Numerical simulation of low-Reynolds-number turbulent flow through a straight square duct. *J. Fluid Mech.* **244**, 101.

GAVRILAKIS, S., TSAI, H. M., VOKE, P. R. & LESLIE, D. C. 1986 Large-eddy simulation of low Reynolds number channel flow by spectral and finite difference methods. *Notes on Numerical Fluid Mechanics* **15**, 105.

GREENSPAN, H.P. 1968 *The Theory of Rotating Fluids.* Cambridge University Press.

JOHNSTON, J. P., HALLEEN, R. M. & LEZIUS, D. K. 1972 Effects of spanwise rotation on the structure of two-dimensional fully developed turbulent channel flow. *J. Fluid Mech.* **56**, 533.

KIM, H. T., KLINE, S. J. & REYNOLDS, W. C. 1971 The production of turbulence near a smooth wall in a turbulent boundary layer. *J. Fluid Mech.* **50**, 133.

KIM, J., MOIN, P. & MOSER, R. 1987 Turbulence statistics in fully developed channel flow at low Reynolds number. *J. Fluid Mech.* **177**, 133.

KRISTOFFERSEN, R. & ANDERSSON, H. I. 1993 Direct simulations of low-Reynolds-number turbulent flow in a rotating channel. *J. Fluid Mech.* **256**, 163.

KRISTOFFERSEN, R., BECH, K. H. & ANDERSSON, H. I. 1993 Numerical study of turbulent plane Couette flow at low Reynolds number. *Appl. Sci. Res.* **51**, 337.

LEE, M. J. & KIM, J. 1991 The structure of turbulence in a simulated plane Couette flow. In *Proc. 8th Symp. on Turbulent Shear Flows*, Munich.

LEZIUS, D. K. & JOHNSTON, J. P. 1976 Roll-cell instabilities in rotating laminar and turbulent channel flows. *J. Fluid Mech.* **77**, 153.

LUMLEY, J. L. 1978 Computational modeling of turbulent flows. *Adv. Appl. Mech.* **18**, 123.

METAIS, O., YANASE, S., FLORES, C., BARTELLO, P. & LESIEUR, M. 1992 Reorganization of coherent vortices in shear layers under the action of solid-body rotation. In *Turbulent Shear Flows VIII*, p. 415. Springer.

MOSER, R. D. & MOIN, P. 1987 The effect of curvature in wall-bounded turbulent flows. *J. Fluid Mech.* **175**, 479.

PAPAVASSILIOU, D. V. 1993 Direct numerical simulation of plane Couette flow. MS thesis, University of Illinois, Urbana-Champaign.

SMITH, G. P. & TOWNSEND, A. A. 1982 Turbulent Couette flow between concentric cylinders at large Taylor numbers. *J. Fluid Mech.* **123**, 187.

SPEZIALE, C. G. & WILSON, M. B. 1989 Numerical study of plane Couette flow in a rotating framework. *Acta Mech.* **77**, 261.

WATMUFF, J. H., WITT, H. T. & JOUBERT, P. N. 1985 Developing turbulent boundary layers with system rotation. *J. Fluid Mech.* **50**, 133.